CHAPTER 5

BEAM-WAVE INTERACTION ANALYSIS FOR BI-FREQUENCY MILO*

*Part of this work has been published as:

Arjun Kumar, Prabhakar Tripathi, Smrity Dwivedi, and Pradip Kumar Jain, "Beam-Wave interaction analysis of an azimuthally partitioned axially periodic metal disc loaded coaxial structure for bi-frequency MILO," *IEEE Transaction on Plasma Science,* vol. 49, no. 4, pp. 1323-1332, April 2021.

5.1. Overview

In this chapter, the electromagnetic behavior of the azimuthally partitioned axially periodic metal disc loaded coaxial structure in the presence of an electron beam using an equivalent circuit approach have been studied. In the analysis, the linearized maxwell's fluid equation (also known as Vlasov-Maxwell's equation) has been used in the electron beam-present region. The effect of all the harmonics presents within the structure has been considered to obtain the expression for the equivalent series inductance per unit length and the equivalent shunt capacitance per unit length for the equivalent transmission line in the presence and absence of an electron beam. The expression for the dispersion relation and the temporal growth rate has been obtained with the help of the calculated equivalent series inductance and equivalent shunt capacitance. The estimation for output RF power and energy has been calculated analytically and the result has been validated through the PIC simulation. The comparison of obtained average power has been compared with the results given in the literature. The relative error between them is below 5% which shows a good agreement. Furthermore, the effect of the different beam parameters on the temporal growth rate behavior has been analyzed.

5.2. Introduction

In recent years, it is noticed that the research activity in the high power microwave (HPM) sources which is capable to generate multi-frequency is drastically increased due to its potential application in the field of defense application, plasma heating, and linear particle accelerator [Benford *et al.* (2007)]. Various HPM sources, such as magnetically insulated line oscillator (MILO), relativistic backward wave oscillator (RBWO), and transit time oscillator (TTO) have been developed to generate bi-frequency RF signals

[Wang *et al.* (2010), Tang *et al.* (2012) and He *et al.* (2011)]. These HPM sources can generate RF power in two or more than two frequencies, either in single-band or dual-band. The single-band bi/tri-frequency devices generate RF power in two/three different frequencies that lie in the same band, while in the case of dual-band devices, the RF power is generated at the two or more frequencies which lie in the different band of frequency. The single-band bi-frequency devices are designed with the help of the azimuthally varying beam wave interaction structure or by using axially varying beam-wave interaction structure [Wang *et al.* (2010) and Tang *et al.* (2012)]. In general, the dual-band devices are designed by integrating the two same/different devices (i.e. operated in a different band) within the single device such as MILO and coaxial TTO, MILO and Vircator, and MILO and MILO [Xiao *et al.* (2009), Zhang *et al.* (2015) and Ju *et al.* (2014)].

The azimuthally partitioned axially periodic metal disc loaded coaxial waveguide structure type beam wave interaction has the potential to generate two or more stable frequencies within a single-band device [Chen *et al.* (2008)]. The HPM source MILO attracts the researcher due to its self-magnetic insulating property which makes the system lighter and compact [Lemke *et al.* (1997)]. The device also has the potential to generate several GW microwave power at multiple frequencies [Benford *et al.* (2007)]. The azimuthally partitioned bi-frequency magnetically insulated line oscillator (BFMILO) have strategic applications, therefore it is necessary to analyze the RF behavior (i.e. electromagnetic (EM) behavior in the presence of electron beam) of the structure so that the proper energy transfer between the electron beam and EM waves takes place [Chen *et al.* (2008)]. A dispersion relation is an excellent tool for analyzing the RF behavior of the structure because the dispersion relation provides information

about the resonance frequency of the RF interaction structure and also very helpful to understand the effect of various structural parameters of the structure on the dispersion behavior.

There are many kinds of literature available to analyze the beam-wave interaction structure which is based on different techniques; such as Lemke *et al*. uses a linear theory with the thin beam approximation for the coaxial structure having square wave type periodic anode but the main constraint associated with this analysis is limited for only symmetric TM_{0n} mode [Lemke *et al.* (1987)]. Zhang *et al.* had used the modified Rayleigh-Fourier technique to analyze the periodic disc loaded cylindrical waveguide structure with axial and azimuthal corrugations in the absence of electron beam [Zhang *et al.* (2005)]. Sagor *et al.* has used a linear analysis for circular-edge disk-loaded cylindrical waveguide structure which is driven by an annular electron beam [Sagor and Amin (2017)]. Dwivedi *et al.* used a modal matching technique for disc-loaded coaxial structure in the presence of an electron beam and find its temporal growth rate for symmetric TM_{01} mode [Dwivedi and Jain (2012)]. The equivalent circuit analysis was used to analyze the disc-loaded coaxial structure in the absence of an electron beam for the azimuthally symmetric TM_{0n} modes by Dixit *et al.* [Dixit and Jain (2016)]. Most of the beam-wave interaction analysis available in the literature are mainly focused on the symmetric modes (i.e. TM modes) and the technique used to analyze the structure involved higher-order matrices which are comparatively difficult to solve and takes a lot of computational time [Lemke *et al.* (1987), Zhang *et al.* (2005), Sagor and Amin (2017) and Dwivedi and Jain (2012)]. In this analysis, the equivalent circuit technique has been selected to analyze the RF behavior of the structure which is found much simpler to handle and is less involved and cumbersome compared with other techniques. In the

azimuthally partitioned axially periodic discs loaded coaxial waveguide structure the EM field distributions generated within the structure exhibit both axial and azimuthal harmonics, so individual TE or TM mode does not exists and therefore hybrid modes (HEM modes) are obtained. Since the EM eigenmodes within the device having all the six components of EM fields, thereby in this analysis we have considers both types of modes (i.e. symmetric and asymmetric mode) for beam-wave interaction.

This research work is arranged in this chapter in this way that Section-5.3 includes the analysis of the beam wave interaction structure (i.e. azimuthally partitioned periodic discs loaded coaxial structure) in the presence of electron beam with the help of equivalent circuit approach. The effect of different structural parameters on the dispersion behavior, temporal growth rate (TGR), RF power, and energy also studied in this section. In the Section-5.4, the computed results obtained using the developed analysis is compared with the simulation for the validation of the developed analysis. The effect of different beam parameters on its TGR associated with the different modes is also presented in this section. Finally, the conclusion of this study is presented in Section-5.5.

5.3. Analysis

The beam-wave interaction analysis for bi-frequency generation inside a MILO device has been performed using an equivalent circuit approach. For this, an azimuthally partitioned axially periodic metal disc loaded coaxial structure (in the presence of electron beam), which is shown in Fig. 5.1, has been used as an interaction structure. Figs. 5.1(a) and 5.1(b) shows the sectional view and front view of the interaction structure, respectively. The geometry of the interaction structure consists of a cylindrical

metal conductor at the center (i.e. used as a cathode), and the two half-cylindrical waveguides have different wall radius (i.e. one half of the cylinder continuous from $0^{\circ} \le \theta \le 180^{\circ}$ with wall radius (i.e. r_{w2}), while other from $180^{\circ} \le \theta \le 360^{\circ}$ with wall radius (i.e. r_{w1})). The parameters associated with the structure are r_c, r_e, r_d, r_{w1}, r_{w2}, L, and T, which indicates the cathode radius, beam radius, inner disc radius, wall radius of azimuthal section-1, wall radius of azimuthal section-2, periodicity and thickness of the disc, respectively. The interaction structure is divided into four regions i.e. region-*I* (i.e. between the cathode to the beam radius, $r_c \le r \le r_e$), region-*II* (between the beam radius to the tip of the metal disc, $r_e \le r \le r_d$), region-*III* (between the tip of the metal disc to wall radius, $r_d \le r \le r_{w1}$, $180^{\circ} \le \theta \le 360^{\circ}$), and region-*IV* ($r_{w1} \le r \le r_{w2}$, $0^{\circ} \le \theta \le 180^{\circ}$). The superscript *I*, *II*, *III*, and *IV*, associated with the different parameter indicates that the parameter belongs to the regions *I*, *II*, *III*, and *IV*, respectively.

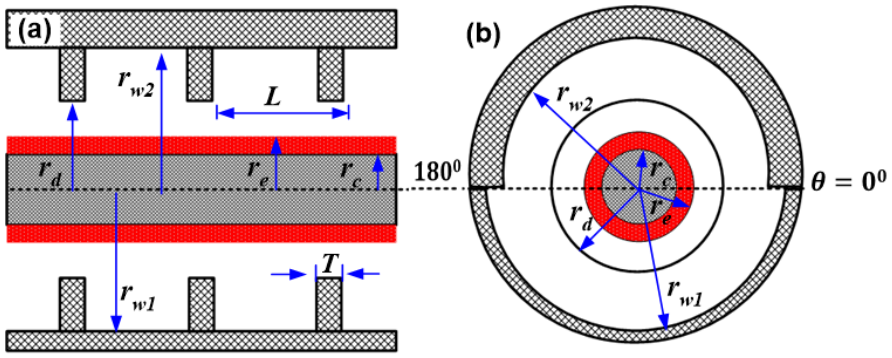

Figure 5.1: Schematic of an azimuthally partitioned axially periodic metal disc loaded coaxial structure with beam-present in red color: (a) sectional view (b) front view.

The beam-wave interaction analysis of the device mainly focuses on determining the dispersion relation (in presence of electron beam) and temporal growth rate along with the estimation of RF output power and energy [Lemke *et al.* (1997), Lemke *et al.*

(1987), and Dwivedi and Jain (2012)]. The dispersion relation and temporal growth rate are determined with the assumption that a para potential flow equilibrium establishes in region-*I* resulting in the generation of the space-charge waves [Lemke and Clark (1987)]. The space charge wave near the anode section (i.e. near the tip of the periodically loaded disc (r_d)) mainly takes part in the beam-wave interaction and induces RF. It is further assumed that region-*II* supports the traveling wave which is influenced by the space charge wave generated in region-*I* while region-*III* and region-*IV* support the standing waves. In order to obtain the field components in region-*I*, Maxwell's fluid equation also known as Vlasov-Maxwell's equation is used. In region-*I* and *II*, the space harmonics effect of the traveling wave is present due to the axial periodicity of the structure (i.e. Floquet's theorem) while the modal harmonics of the standing wave are present in the regions-*III* and *IV* due to the reflections of EM waves from the metallic surfaces. Since the structure is periodic in the axial (z) direction as well as periodic in the azimuthal (θ) direction, the pure TE or TM mode does not exist in the structure. In place of symmetrical TE and TM modes, the structure supports the asymmetrical modes (i.e. HEM mode). The field components in the different structure regions can be derived as following [Lemke and Clark (1987)]:

5.3.1. EM Field Expression in the Presence of Electron Beam

The Vlasov-Maxwell's equation for TM mode (i.e. $H_z = 0$) is given as [Dwivedi and Jain (2012) and Lemke (1989)]:

$$\left(\frac{\partial}{\partial t} + v_z \frac{\partial}{\partial z}\right) P_z = -eE_z, \tag{5.1}$$

$$\frac{1}{r}\frac{\partial}{\partial r}(rE_r)+\frac{\partial E_z}{\partial z}=-4\pi e n_e, \tag{5.2}$$

$$\frac{\partial E_r}{\partial z}-\frac{\partial E_z}{\partial r}=-\frac{1}{c}\frac{\partial B_\theta}{\partial t}, \tag{5.3}$$

$$-\frac{\partial B_\theta}{\partial z}=\frac{1}{c}\frac{\partial E_r}{\partial t}, \tag{5.4}$$

$$\frac{1}{r}\frac{\partial (rB_\theta)}{\partial z}=\frac{4\pi}{c}J_z+\frac{1}{c}\frac{\partial E_z}{\partial t}. \tag{5.5}$$

Here, $P_z=\gamma m v_z$ is the axial momentum, $\gamma=1/(1-v_z^2/c^2)^{1/2}$ is the relativistic factor, $J_z=-\eta e n_e v_z \delta(r-r_e)$ is the axial current density, n_e is the charge number density, v_z is the axial drift velocity, $\delta(r-r_e)$ is the delta function, and r_e is the electron beam radius. The parameter η is the normalized factor determined by, $\eta=|I_e|/(2\pi e r_e n v_z)$. Solving the above equation, the electric and magnetic field components for TM modes is derived as:

$$E_{r,n}=i\frac{\beta_n}{\gamma_n^2}\frac{dE_{z,n}}{dr}, \tag{5.6}$$

$$B_{\theta,n}=i\frac{\omega/c}{\gamma_n^2}\frac{dE_{z,n}}{dr}, \tag{5.7}$$

$$\left(\frac{1}{r}\frac{d}{dr}r\frac{d}{dr}+\gamma_n^2\right)E_{z,n}=\frac{\alpha c^2}{(\pi/2)r_e}\frac{\gamma_n^2 E_{z,n}}{(\omega-v_z\beta_n)^2}\delta(r-r_e). \tag{5.8}$$

Here, $\gamma_n^2=\omega^2/c^2-\beta_n^2$ is the radial propagation constant, and $\alpha=\pi|I_e|/(\gamma_n^2 I_A)$ with $I_A=17.1\gamma v_z/c$ kA is the Alfven current.

Similar to the TM mode derived above, Maxwell's fluid equation for the TE mode is derived as:

$$\left(\frac{\partial}{\partial t}+v_\theta\frac{\partial}{\partial \theta}\right)P_\theta=-eE_\theta, \tag{5.9}$$

$$\frac{1}{r}\frac{\partial E_\theta}{\partial \theta}=-4\pi e n_e \tag{5.10}$$

$$\frac{\partial E_\theta}{\partial z}=\frac{1}{c}\frac{\partial B_r}{\partial t}, \tag{5.11}$$

$$\frac{1}{r}\frac{\partial}{\partial r}(rE_\theta)=-\frac{1}{c}\frac{\partial B_z}{\partial t} \tag{5.12}$$

$$\frac{\partial B_r}{\partial z}-\frac{\partial B_z}{\partial r}=\frac{4\pi}{c}J_\theta+\frac{1}{c}\frac{\partial E_\theta}{\partial t}\quad , \tag{5.13}$$

here, $P_\theta=\gamma m v_\theta$ is the azimuthal momentum, $J_\theta=-\eta e n_e v_\theta \delta(r-r_e)$ is the azimuthal current density, v_θ is the azimuthal drift velocity. For the charge equilibrium condition, $dn_e/dt=0$, which can be expressed as:

$$\frac{\partial n}{\partial t}+\frac{\partial (n v_\theta)}{\partial \theta}=0 \qquad . \tag{5.14}$$

By putting $\frac{\partial}{\partial t}=-i\omega$ and, $\frac{\partial}{\partial \theta}=il$, where l is the azimuthal harmonic number, the above Eqs. (5.9) to (5.14) can be expressed as:

$$B_r=-\frac{\beta_n}{\beta}E_\theta \tag{5.15}$$

$$E_\theta = \frac{\beta}{j\gamma_n^2}\left\{\frac{\partial B_z}{\partial r} + \frac{4\pi}{c} J_\theta\right\} \tag{5.16}$$

$$J_\theta = i\eta \frac{e^2 n_0}{m\gamma_0^3} \frac{\omega E_\theta}{(\omega - v_z\beta_n)^2} \delta(r - r_e) \tag{5.17}$$

$$\left(\frac{1}{r}\frac{d}{dr} r \frac{d}{dr} + \gamma_n^2\right) H_{z,n} = \frac{\alpha c^2}{(\pi/2) r_e} \frac{\gamma_n^2 \beta H_{z,n}}{(\omega - v_z\beta_n)^2} \delta(r - r_e). \tag{5.18}$$

With the calculation of axial electric (E_z) and axial magnetic field (H_z), the four transverse field components can be written using Maxwell's equation as:

$$E_r^{\Re} = \left(\frac{-j}{\gamma_n^2}\right)\left\{\beta_n \frac{\partial E_z^{\Re}}{\partial r} + \frac{\omega\mu}{r}\frac{\partial H_z^{\Re}}{\partial \theta}\right\} \tag{5.19}$$

$$E_\theta^{\Re} = \left(\frac{-j}{\gamma_n^2}\right)\left\{\frac{\beta_n}{r}\frac{\partial E_z^{\Re}}{\partial \theta} - \omega\mu \frac{\partial H_z^{\Re}}{\partial r}\right\} \tag{5.20}$$

$$H_r^{\Re} = \left(\frac{j}{\gamma_n^2}\right)\left\{\frac{\omega\varepsilon}{r}\frac{\partial E_z^{\Re}}{\partial \theta} - \beta_n \frac{\partial H_z^{\Re}}{\partial r}\right\} \tag{5.21}$$

$$H_\theta^{\Re} = \left(\frac{-j}{\gamma_n^2}\right)\left\{\omega\varepsilon \frac{\partial E_z^{\Re}}{\partial r} - \frac{\beta_n}{r}\frac{\partial H_z^{\Re}}{\partial \theta}\right\} \quad . \tag{5.22}$$

Here, superscript $\Re$ stands for region-*I*, *II*, *III*, and *IV* for corresponding regions. The electric and magnetic field components in different regions are given as:

(i). Region-*I* (i.e. $r_c \le r \le r_e$)

$$E_z^I = \sum_{\upsilon=-\infty}^{\infty}\sum_{n=-\infty}^{\infty} (k^2 - (\beta_n)^2)\{J_\upsilon(\gamma_n^* r) Y_\upsilon(\gamma_n^* r_c) - Y_\upsilon(\gamma_n^* r) J_\upsilon(\gamma_n^* r_c)\} A_{\upsilon,n}^* \times \exp(-i(\beta_n z + \upsilon\theta))$$

(5.23)

$$H_z^I = \sum_{\upsilon=-\infty}^{\infty}\sum_{n=-\infty}^{\infty}(k^2-(\beta_n)^2)\{J_\upsilon(\gamma_n^* r)Y_\upsilon'(\gamma_n^* r_c)-Y_\upsilon(\gamma_n^* r)J_\upsilon'(\gamma_n^* r_c)\}B_{\upsilon,n}^* \times \exp(-i(\beta_n z+\upsilon\theta))$$

.

(5.24)

Here, $\beta_n = \beta_0 + 2n\pi/L$ is the axial propagation constant; γ_n^* is the radial propagation constant in presence of electron beam i.e. $(\gamma_n^*)^2 = \gamma_n^2\left(1-\frac{\alpha c^2}{(\pi/2)r_e(\omega-v_z\beta_n)^2}\delta(r-r_e)\right)$ and $((\gamma_n)^2 = k^2-(\beta_n)^2)$, $A_{\upsilon,n}^*$, $B_{\upsilon,n}^*$ is the undetermined coefficient; $n = 0,\pm1,\pm2,\pm3,...,$ $\upsilon = 0,\pm1,\pm2,\pm3,...,$ J_υ and Y_υ is the Bessel function of 1st and 2nd kind of order υ.

(ii). Region-*II* (i.e. $r_e \le r \le r_d$)

The field component in this region is obtained by applying the boundary condition between an electron beam and vacuum region similar to the literature [Lemke (1989)] and expressed as:

$$E_z^{II} = \sum_{\upsilon=-\infty}^{\infty}\sum_{n=-\infty}^{\infty}(k^2-(\beta_n^I)^2)U_{\upsilon,n}^*(r)A_{\upsilon,n}^* \times \exp(-i(\beta_n z+\upsilon\theta)) \tag{5.25}$$

$$H_z^{II} = \sum_{\upsilon=-\infty}^{\infty}\sum_{n=-\infty}^{\infty}(k^2-(\beta_n)^2)V_{\upsilon,n}^*(r)B_{\upsilon,n}^* \times \exp(-i(\beta_n z+\upsilon\theta)) \quad , \tag{5.26}$$

here, $U_{\upsilon,n}^*(r)$, and $V_{\upsilon,n}^*(r)$, are represented by the Bessel function as,

$$\begin{aligned} U_{\upsilon,n}^*(r) = {} & Y_\upsilon(\gamma_n r_c)J_\upsilon(\gamma_n r) - J_\upsilon(\gamma_n r_c)Y_\upsilon(\gamma_n r) \\ & -\alpha[c^2\gamma_n^2\psi_n/(\omega-\beta_n v_z)^2]\times[Y_\upsilon(\gamma_n r_e)J_\upsilon(\gamma_n r) - J_\upsilon(\gamma_n r_e)Y_\upsilon(\gamma_n r)] \end{aligned} \tag{5.27}$$

$$V_{\upsilon,n}^{*}(r) = Y_{\upsilon}'(\gamma_n r_c)J_{\upsilon}(\gamma_n r) - J_{\upsilon}'(\gamma_n r_c)Y_{\upsilon}(\gamma_n r) - \alpha[c^2\gamma_n^2\beta^2\zeta_n / (\omega - \beta_n v_\theta)^2] \times [Y_{\upsilon}'(\gamma_n r_e)J_{\upsilon}(\gamma_n r) - J_{\upsilon}'(\gamma_n r_e)Y_{\upsilon}(\gamma_n r)] \quad . (5.28)$$

(iii). Region-*III* (i.e. $r_d \le r \le r_{w1}$**)**

Similar to the field expression for the disc occupied regions explained in the literature [Wang *et al.* (2016)], the axial electric and axial magnetic field can be express as:

$$E_z^{III} = \sum_{\upsilon=-\infty}^{\infty}\sum_{m=1}^{\infty}(k^2 - (\beta_m)^2)[J_{\upsilon}(\gamma_m r)A_{\upsilon,m}^{III} + Y_{\upsilon}(\gamma_m r)B_{\upsilon,m}^{III}] \times \sin(\beta_m z)\exp(-i\upsilon\theta) \quad (5.29)$$

$$H_z^{III} = \sum_{\upsilon=-\infty}^{\infty}\sum_{m=1}^{\infty}(k^2 - (\beta_m)^2)[J_{\upsilon}(\gamma_m r)C_{\upsilon,m}^{III} + Y_{\upsilon}(\gamma_m r)D_{\upsilon,m}^{III}] \times \cos(\beta_m z)\exp(-i\upsilon\theta) \quad . \quad (5.30)$$

Here, $\beta_m = m\pi / d$, is the propagation phase constant in region-*III*, $(\gamma_m)^2 = k^2 - (\beta_m)^2$ is the radial propagation constant in region-*III*; $m = 1, 2, 3, ...$; $A_{\upsilon,m}^{III}$, $B_{\upsilon,m}^{III}$, $C_{\upsilon,m}^{III}$, $D_{\upsilon,m}^{III}$ are the unknown coefficients.

(iv). Region-*IV* (i.e. $r_{w1} \le r \le r_{w2}, 180^\circ \le \theta \le 360^\circ$ **)**

$$E_z^{IV} = \sum_{s=1}^{\infty}\sum_{m=1}^{\infty}\left(k^2 - (\beta_m)^2\right)U_{s,m}(r)A_{s,m}^{IV} \times \sin(\beta_m z)\sin(s\theta) \quad (5.31)$$

$$H_z^{IV} = \sum_{s=1}^{\infty}\sum_{m=1}^{\infty}\left(k^2 - (\beta_m)^2\right)V_{s,m}(r)B_{s,m}^{IV} \times \cos(\beta_m z)\cos(s\theta) \quad . \quad (5.32)$$

Here $A_{s,m}^{IV}$, $B_{s,m}^{IV}$ is the undetermined coefficient; $U_{s,m}$ and $V_{s,m}$ represented by a Bessel function as:

$$U_{s,m}(r) = Y_s(\gamma_m r_{w2})J_s(\gamma_m r) - J_s(\gamma_m r_{w2})Y_s(\gamma_m r) \quad (5.33)$$

$$V_{s,m}(r) = Y_s'(\gamma_m r_{w2}) J_s(\gamma_m r) - J_s'(\gamma_m r_{w2}) Y_s(\gamma_m r) \quad . \tag{5.34}$$

5.3.2 Boundary condition

The boundary condition of the electromagnetic field satisfies the boundary condition between the region-*II* and the region-*III* (*i.e.* at, $r = r_d$) are:

$$E_z^{II} = \begin{cases} E_z^{III} & (0 \le z \le (L-T)), \quad r = r_d \\ 0 & ((L-T) \le |z| \le L), \quad r = r_d \end{cases} \tag{5.35}$$

$$E_\theta^{II} = \begin{cases} E_\theta^{III} & (0 \le z \le (L-T)), \quad r = r_d \\ 0 & ((L-T) \le |z| \le L), \quad r = r_d \end{cases} \tag{5.36}$$

$$H_z^{II} = H_z^{III} \qquad (0 \le z \le (L-T)), \tag{5.37}$$

$$H_\theta^{II} - H_\theta^{III} = I_z / 2\pi r_d \qquad (0 \le z \le (L-T)), \tag{5.38}$$

$$E_r^{III} - E_r^{II} = \rho_s / \varepsilon \qquad (0 \le z \le (L-T)), \tag{5.39}$$

here, I_z is the axial current flowing near the tip of the disc and ρ_s is the surface charge density at the discontinuity interface of region *II* and region *III*.

The boundary condition of the electromagnetic field satisfies the boundary condition between region *III*, and region *IV* (*i.e.* at, $r = r_{w1}$ and $0^0 \le \theta < 180^0$ are:

$$E_z^{III} = \begin{cases} E_z^{IV} & (0^\circ \le \theta \le 180^\circ), \\ 0 & (180^\circ \le \theta \le 360^\circ), \end{cases} \tag{5.40}$$

$$E_{\theta}^{III} = \begin{cases} E_{\theta}^{IV} & (0^{\circ} \le \theta \le 180^{\circ}), \\ 0 & (180^{\circ} \le \theta \le 360^{\circ}), \end{cases} \tag{5.41}$$

$$H_{z}^{III} = H_{z}^{IV} \qquad (0^{\circ} \le \theta \le 180^{\circ}), \tag{5.42}$$

$$H_{\theta}^{III} = H_{\theta}^{IV} \qquad (0^{\circ} \le \theta \le 180^{\circ}). \tag{5.43}$$

After applying the above boundary conditions between region-*III* and *IV*, we can represent the coefficient of region-*IV* in terms of the coefficient of region-*III*, similarly, the boundary condition between region-*III* and region-*II* helps to express the coefficient of region-*III* in the form of the coefficient of region-*II* (i.e. in terms of A_n^*) as described in the previous chapter (i.e. chapter 4). Thus, $B_{\upsilon,m}^{III} = G_{B,A}^{*} A_{\upsilon,m}^{III}$, $C_{\upsilon,m}^{III} = G_{C,A}^{*} A_{\upsilon,m}^{II}$, $D_{\upsilon,m}^{III} = G_{D,A}^{*} A_{\upsilon,m}^{III}$ and $A_{\upsilon,m}^{III}$ can be express as:

$$A_{\upsilon,m}^{III} = \sum_{n=-\infty}^{\infty} M_{n,m}^{*} A_{\upsilon,n}^{*} \quad , \tag{5.44}$$

here, $G_{B,A}^{*}$, $G_{C,A}^{*}$ and $G_{C,A}^{*}$ is the transformation expression as explained in the previous chapter 4, and $M_{n,m}^{*} = \dfrac{(k^2 - (\beta_n)^2) U_{\upsilon,n}^{*}(r_d)}{(k^2 - (\beta_m)^2)\{J_{\upsilon}(\gamma_m r_d) + G_{B,A}^{*} Y_{\upsilon}(\gamma_m r_d)\}} \left(\dfrac{\bar{S}_1}{L} \right)$, with $\bar{S}_1 = \int_0^{L-T} \sin(\beta_m z) e^{-i\beta_n z} dz$.

5.3.3 Dispersion Relation

Using the current telegraphist's equation, the capacitance per unit length defined for azimuthal partition disc loaded coaxial structure in the presence of an electron beam and can be express as:

$$(C_e^*)_\upsilon = \frac{j(\gamma_n)^2}{\omega}\frac{1}{P^*_{\upsilon,nm}} \quad , \tag{5.45}$$

here, $P^*_{\upsilon,nm} = \sum_{n=-\infty}^{\infty} \frac{R^*_{\upsilon,nm}(k^2-(\beta_n)^2)U^*_{\upsilon,n}(r_d)\bar{S}_1}{2\pi r_d}$ and,

$$R^*_{\upsilon,nm} = \sum_{m=1}^{\infty}[i\omega\varepsilon\gamma_n U'^*_{\upsilon,n}(r_d) - \frac{i\omega\varepsilon\beta_m(L-T)\gamma_m M^*_{n,m}}{2}\{J'_\upsilon(\gamma_m r_d) + G^*_{B,A}Y'_\upsilon(\gamma_m r_d)\}$$
$$- \frac{i\upsilon\varepsilon M^*_{n,m}(J_\upsilon(\gamma_m r_d)G^*_{C,A} + Y_\upsilon(\gamma_m r_d)G^*_{D,A})}{r_d}\{\frac{\beta_m(L-T)}{2} - \frac{i\beta_n(k^2-(\beta_m)^2)\bar{S}_1}{2(k^2-(\beta_n)^2)}\}]^{-1}$$

Similarly, using voltage telegraphist's equation, the inductance per unit length defined for azimuthal partition disc loaded coaxial structure in the presence of an electron beam and can be express as:

$$(L_e^*)_\upsilon = \frac{1}{j\omega}\left(\frac{\beta_n}{\gamma_n}\right)^2 \times \frac{1}{W^*_{\upsilon,nm}} \quad , \tag{5.46}$$

here, $W^*_{\upsilon,nm} = \sum_{n=-\infty}^{\infty} \frac{Q^*_{\upsilon,nm}U^*_{\upsilon,n}(r_d)\bar{S}_1}{2\pi r_d}$ and,

$$Q^*_{\upsilon,nm} = \sum_{m=1}^{\infty}[i\beta_n\gamma_n\omega\mu U^*_{\upsilon,n}(r_d) - \frac{\upsilon\omega\mu(k^2-(\beta_m)^2)S_2\left(J_\upsilon(\gamma_m r_d)G^*_{C,A} + Y_\upsilon(\gamma_m r_d)G^*_{D,A}\right)}{r_d(L-T)(k^2-(\beta_n)^2)}]^{-1}$$

The dispersion relation in the presence of electron beam for different modes can be obtained in the form of structure parameters using the equivalent shunt capacitance per unit length ($(C_e^*)_\upsilon$) and equivalent series inductance per unit length ($(L_e^*)_\upsilon$) and express as:

$$\beta^2 - \omega^2(L_e^*)_\upsilon(C_e^*)_\upsilon = 0 \quad . \tag{5.47}$$

After rearranging the above expression (i.e. Eqs. (5.47)), the dispersion relation in presence of an electron beam can be express as:

$$\sum_{\upsilon=-\infty}^{\infty}\sum_{n=-\infty}^{\infty}\sum_{s=1}^{\infty}\sum_{m=1}^{\infty}\left[\frac{\beta_0\gamma_n U'^{*}_{\upsilon,n}(r_d)U_{s,m}(r_d)}{(\beta_0^2-\beta_n^2)U^{*}_{\upsilon,n}(r_d)U'_{s,m}(r_d)}-\frac{\upsilon^2\beta_n^2 V^{*}_{\upsilon,n}(r_d)U_{s,m}(r_d)}{\beta_0\gamma_n r_d^2(\beta_0^2-\beta_n^2)V'^{*}_{\upsilon,n}(r_d)U'_{s,m}(r_d)}\right]\times \times\frac{(L-T)}{L}\frac{\sin^2\left(\beta_n(L-T)/2\right)}{\left(\beta_n(L-T)/2\right)^2}=0 \quad (5.48)$$

5.3.4 Temporal growth rate

In the presence of an electron beam, the roots of dispersion relation explained in the above section (i.e. Eq. (5.48)) results in complex roots of frequency for a range of wavenumber. This range of wavenumber is mainly called the instability region and is considered as the region between the cutting point of beam-line (i.e. defined as $\omega=\beta_0 v_e$) and slow space charge wave (slow SCW) line on dispersion curve [Dwivedi and Jain (2012) and Lemke (1989)]. The beam-line is defined by $\omega=\beta_0 v_e$, here, v_e is the maximum electron velocity. The slow SCW is defined by [Lemke (1989)], $\omega=\beta_0 v_{\text{slow\_sc}}$, here, $v_{\text{slow\_sc}}=v_e\left(1-\omega_p/(\omega_c\gamma_0^{1.5})\right)$. In the instability region, the slow SCW interacts with the RF wave supported by the structure and produce real as well as imaginary roots of frequency. The real root of frequency (i.e. f_r) gives the oscillation frequency of RF wave whereas the imaginary root of frequency (i.e. f_i) gives the temporal growth rate (i.e. rate at which the oscillation frequency grows with time in the instability region). To find the magnitude of the temporal growth rate, the imaginary value of frequency (i.e. f_i) is calculated using Eq. (5.48). This imaginary frequency causes the exponential grow of RF

(i.e. $e^{-i2\pi(f_r+if_i)t}$) with the increase in time [Sagor and Amin (2017)].

5.3.5. RF energy and Power

In this section, the estimated RF output power and stored RF energy associated with two different fundamental frequencies for bi-frequency MILO is calculated using an equivalent circuit approach. To eliminate the complication, the estimated RF energy stored inside the azimuthal partition disc-loaded coaxial structure is calculated for two different fundamental frequencies associated with the different azimuthal cavity. The equivalent admittance for cavity formed with disc loaded coaxial structure can be calculated as [Dixit (2016)]:

$$Y(\omega) = \frac{1}{R}\left[1 + jQ_{\text{int}}\left(\frac{\omega}{\omega_0} - \frac{\omega_0}{\omega}\right)\right] \quad . \tag{5.49}$$

Here, $Q_{\text{int}} = RC\omega_0$ represents an internal quality factor of a cavity, due to dissipative losses in the walls and $Q_{ext} = Z_0 / \omega_0 L = Z_0 C\omega_0$ is the external quality factor with Z_0 represents the output impedance of the signal source [Cousin (2005)]. The imaginary part of admittance represents energy stored or released from the cavity. In MILO, energy stored inside the cavity is coupled with the load through a coaxial line with the output opening axially [Cousin (2005)]. Interaction cavities coupling with the load may be either over coupling or under coupling depends upon the external and internal Q-factor. The coupling coefficient of the cavity is defined as [Dixit (2016)]:

$$\frac{Q_{ext}}{Q_{\text{int}}} = \frac{Z_0}{R} = \alpha \quad . \tag{5.50}$$

The coupling coefficient for fundamental mode frequency of the cavity can also be

calculated by the ratio of coupling capacitance of the RF cavities and the cavity capacitance and given as:

$$\alpha = \frac{C'}{C_e} \quad , \tag{5.51}$$

Where, C' and C_e defined as the coupling capacitance and fundamental mode capacitance of the cavity given as [Fan *et al.* (2008)]:

$$C' = \frac{2\pi\varepsilon_0 T}{\ln(r_d / r_c)} + 8\varepsilon_0 \left[(L-T) + \left(r_d - \frac{2(r_d - r_c)}{\pi} \right) \ln\left(\frac{\pi(L-T) + 2(r_d - r_c)}{2(r_d - r_c)} \right) \right]$$

and,

$$C_e = 2\varepsilon_0 r_d \ln\left(\frac{(L-T)/2 + T}{(L-T)/2} \right) + \frac{2\pi\varepsilon_0}{3(L-T)(r_w - r_d)} \left(r_w^3 + 2r_d^3 - 3r_w r_d^2 \right) .$$

Now, stored RF energy inside the cavity for two different frequencies can be defined as [Cousin (2005) and Dixit (2016)]:

$$W_a(t) = W_{0,a} \left[1 - \exp\left(-\frac{\omega_{0,a}}{2Q_{0,a}} (t - t_0) \right) \right]^2 \quad , \tag{5.52}$$

here, the subscript a is either *1* or *2* considered for two different modes, t_0 is the initial time, $W_{0,a} (= 4P_0 Q_{0,a}^2 / \omega_{0,a} Q_{ext,a})$ is the stored energy in different frequencies, and P_0 $(= 0.32(I_{s,\max} V_0))$ is the estimated RF output power defined in the literature [Lemke *et al.* (1997)]. The RF output power distributed among the two frequencies can be calculated as [Dixit (2016)]:

$$P_a = \sqrt{\frac{4P_0\omega_{0,a}W_a}{Q_{ext,a}}} - \frac{\omega_{0,a}W_a}{Q_{ext,a}} \quad . \tag{5.53}$$

5.4. Results and discussion

An azimuthally partitioned axially periodic metal disc loaded coaxial structure has been analyzed in the presence of an electron beam using an equivalent circuit approach considering Vlasov-Maxwell's equation. Through the analysis, the potential of the structure to generate two stable and separate frequencies within a single MILO device has been estimated by deriving dispersion relation and temporal growth rate. The dispersion relation is considered as a basic tool to estimate the potential of RF generation and propagation through any slow-wave structure whereas the temporal growth rate is used to estimate the growth of a generation of RF with time. To validate the derived dispersion relation and temporal growth rate, first, the dispersion and temporal growth rate for MILO structure described in the literature [Dwivedi and Jain (2012)] has been calculated and found in perfect match with the reported results.

The dispersion relation derived in Eqs. (5.48) is used for numerical calculation of the dispersion curve of two different modes supported by the different azimuthal section of azimuthally partitioned axially periodic metal disc loaded coaxial structure. Fig. 5.2 shows the dispersion curve for the structure with beam parameters: beam voltage (V=420 kV), beam current (I_a=38 kA) and beam radius ($r_e = 0.85 \times r_d$), and design parameters: different wall radii (r_{w1}= 140 mm and r_{w2}=129 mm), cathode radius (r_c=53 mm), disc inner radius (r_d=86 mm), disc periodicity (L=27 mm) and disc thickness (T=5 mm). The different modes considered here describe as fundamental modes which are responsible for the generation of frequency associated with one part of the azimuthal section (i.e. r_{w1}

=140 mm and azimuthal range 180^0-360^0 (blue color)) and other is responsible for the generation of frequency associated with another part of the azimuthal section (i.e. r_{w2} =129 mm and azimuthal range 0^0-180^0 (brown color)).

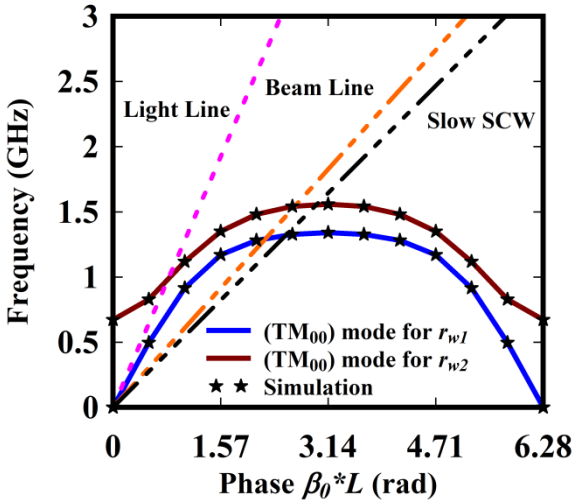

Figure 5.2: Dispersion curve for azimuthally partitioned axially periodic metal disc loaded coaxial structure in presence of beam at voltage V=420 kV, current I_a=38 kA, with different wall radii, r_{w1}= 140 mm and r_{w2}=129 mm (with, r_c=53 mm, r_d=86 mm, L=27 mm and T=7 mm).

The fundamental modes in azimuthally partitioned axially periodic metal disc loaded coaxial structure associated with a different azimuthal section is TM_{00} modes. As the dispersion curve is below the light line, the structure is considered a slow-wave structure. The region between beam-line and slow SCW line is considered as instability region and the temporal growth rate is calculated in this region. Fig. 5.3 shows the temporal growth rate (f_i) at different phases ($\beta_0 * L$) in radian for different modes. It can be seen from Fig. 5.3 that the maximum value of temporal growth rate for TM_{00} mode of section-1 (i.e. of r_{w1}) is ~0.046 per ns and for TM_{00} mode of section-2 (i.e. r_{w2}) is ~0.06

per ns which indicate that frequency associated with f_2 grows faster than that of f_1.

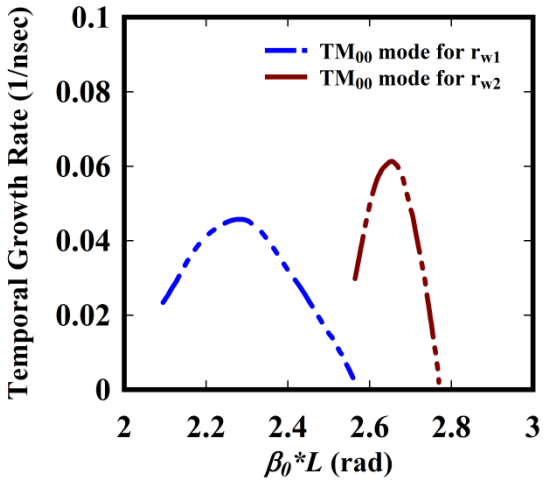

Figure 5.3: Temporal growth rate (f_i) at different phase ($\beta_0 * L$) in radian for two operating modes supported by the structure for two different azimuthal sections (i.e. TM_{00} mode for r_{w1} and TM_{00} mode for r_{w2}).

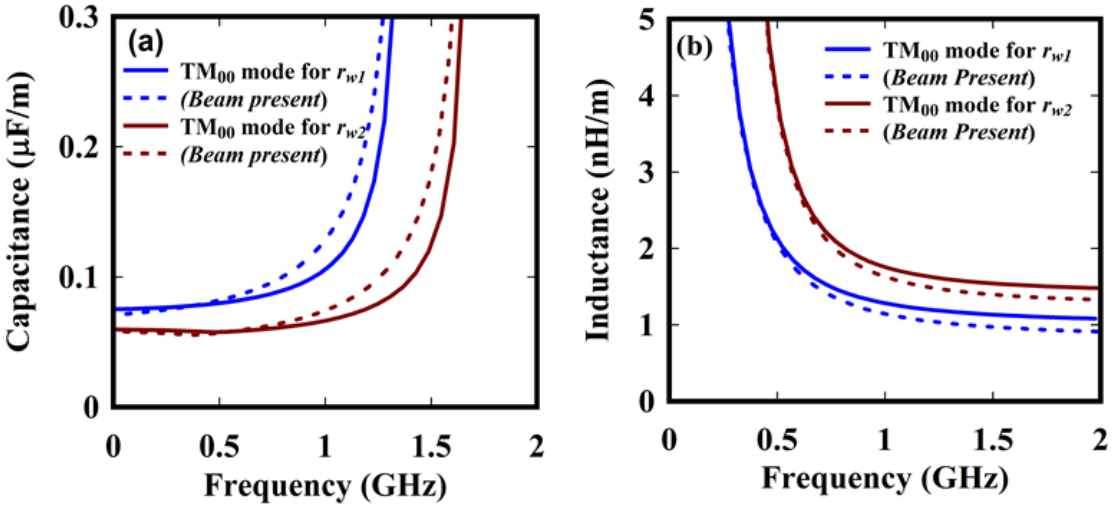

Figure 5.4: Equivalent shunt capacitance and equivalent series inductance of the transmission line in the presence and absence of electron beam: (a) Shunt capacitance per unit length (b) Series inductance per unit length.

The equivalent shunt capacitance and series inductance per unit length of the equivalent transmission line in the presence and absence of electron beam for the two modes associated with the azimuthally partitioned structure are numerically calculated and shown in Fig. 5.4. The shunt capacitance per unit length is shown in Fig. 5.4(a) and it can be seen from the figure that the shunt capacitance per unit length for two resonating modes in the presence of electron beam shifted slightly left representing beam loading effect. Fig. 5.4(b) shows series inductance per unit length. A similar effect is also observed for the series inductance per unit length which is shown in Fig. 5.4(b).

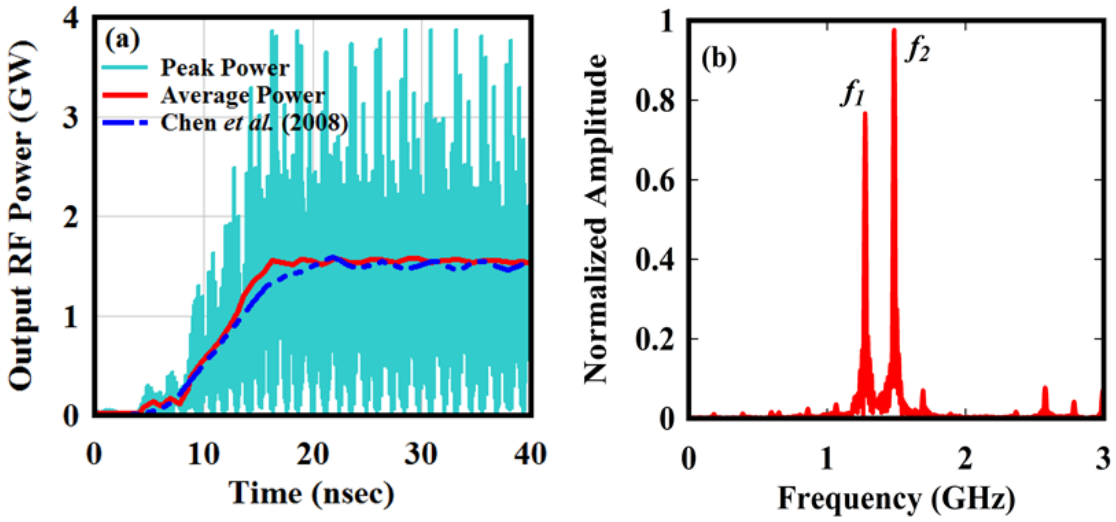

Figure 5.5: (a) RF output peak and average powers obtained through simulation and comparison with reported results [Chen *et al.* (2008)] (b) FFT of generated RF signal of the designed bi-frequency MILO considering azimuthally partitioned axially periodic metal disc loaded coaxial structure as interaction structure.

The estimation of RF power generated through the beam-wave interaction in azimuthally partitioned axially periodic metal disc loaded coaxial structure is expressed in Eqs. (5.53). To validate the RF generation at two frequencies in a single MILO device,

the azimuthally partitioned axially periodic metal disc loaded coaxial structure which is used as an interaction structure has been simulated in the presence of an electron beam through commercially available software 'CST studio suite'. The output RF peak and average power generated through the device and the FFT of the RF signal is shown in Fig. 5.5 along with the comparison of results given in the literature [Chen *et al.* (2008)]. It can be seen from Fig. 5.5(a) that almost 1.3 GW of average RF power is obtained through simulation and the FFT of the obtained RF signal given in Fig. 5.5(b) shows that

signal oscillates at two frequencies (i.e. f_1=1.27 GHz and f_2=1.49 GHz). It can also be seen from Fig. 5.5(b) that, the magnitude of frequency (f_1) is smaller than the magnitude of frequency (f_2) which validates the above discussed temporal growth rate where f_1 has a slower growth rate than that of f_2. Furthermore, to validate the above describe analysis, the obtained results (i.e. RF output power and associated energy) through analysis are compared with simulation results and shown in Fig. 5.6. It is observed that the obtained results (i.e. through analysis) are in close agreement (i.e. error within ~5%) with the simulation results. Fig. 5.6(a) shows the average RF output power obtained through analysis and simulation. The maximum energy stored inside the cavity associated with the RF signal calculated with the time integration of average power (i.e. shown in Fig. 5.6(a)) and found ~50 J. To investigate the temporal behavior of energy distribution inside the cavity, the above describe Eqs. (5.52) is used. In the analytical calculated RF power and energy, the consideration of magnetic insulation is taken as ideal, therefore, the RF power generation starts early as compare to the simulation. Fig. 5.6(b) shows the normalized energy associated with RF signal at different time instant obtained through analysis and simulation.

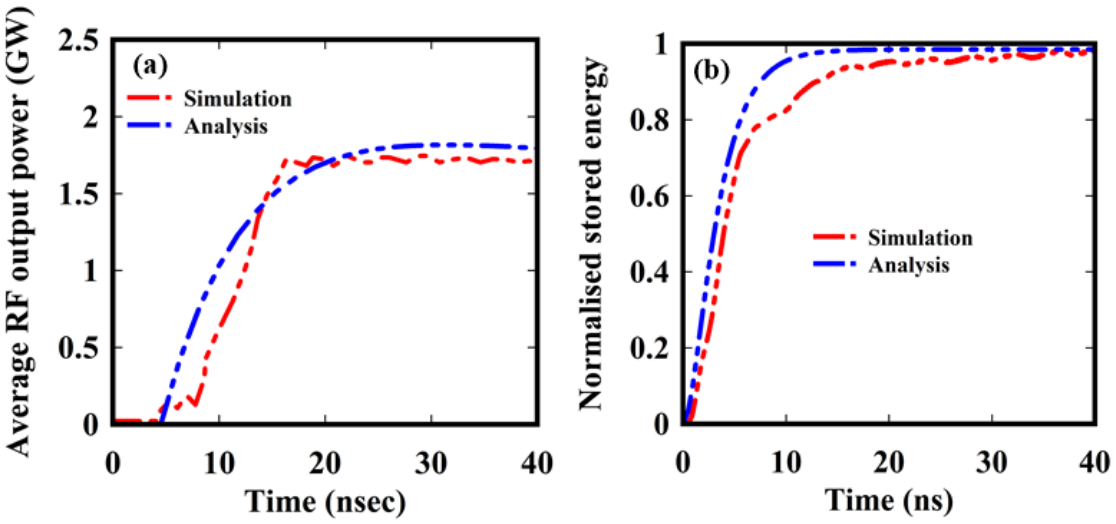

Figure 5.6: Comparison of obtained analytical results with simulation results (a) Average RF output power with time, (b) Normalized energy store in the cavity with time.

5.4.1 Effect of variation of beam parameters

The effect of beam parameter variation on the temporal growth rate for two different modes associated with the azimuthal partitioned axially periodic disc loaded coaxial structure in the presence of an electron beam is shown in Fig. 5.7. Figs. 5.7(a) and 5.7(b) depict the sensitivity of the variation of input beam voltage (V) and beam radius (r_e) on the operating modes. Fig. 5.7(a) shows that with the increase in input beam voltage (V), the temporal growth rate shifted slightly left because of the shifting of the effective beamline. The shifting of beam-line towards left also decreases the effective beam-wave interaction with an increase of input beam voltage thus resulting decrease in the maximum value of temporal growth rate. Fig. 5.7(b) shows that with the decrease of beam radius (r_e), the temporal growth rate decrease as the maximum beam-wave interaction takes place at the tip of the loaded disc.

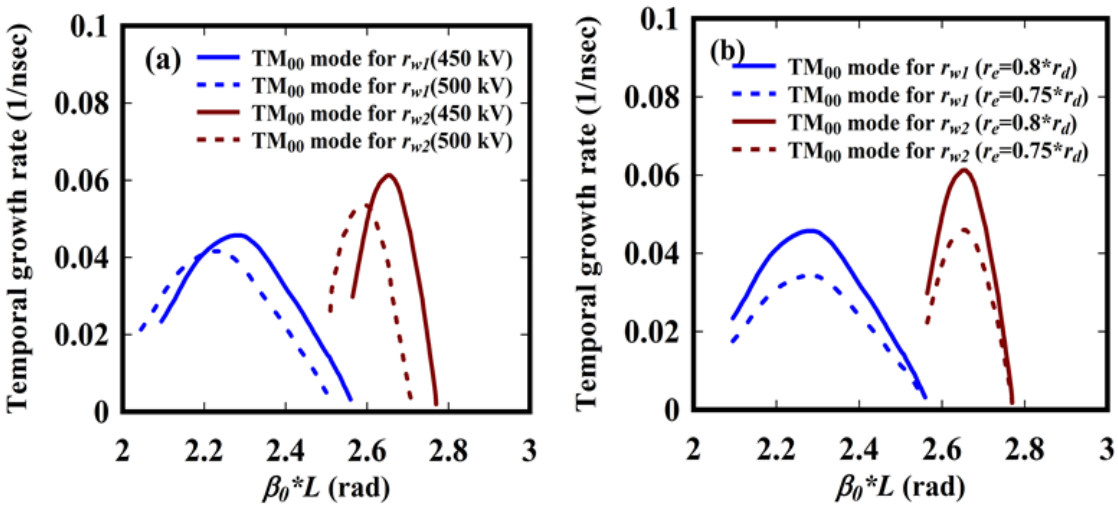

Figure 5.7: Effect of beam parameters on the temporal growth rate of the azimuthally partitioned axially periodic disc loaded coaxial structure in the presence of electron beam: (a) different input beam voltage (V), (b) different beam radius (r_e).

5.5 Conclusion

In this chapter, we have performed the electron beam present analysis for an azimuthally partitioned axially periodic metal disc loaded coaxial structure which can be used as the MILO RF interaction structure for the bi-frequency HPM generation. The structure is analyzed using the equivalent circuit approach which is found much simpler, less cumbersome. The expression for equivalent capacitance per unit length and equivalent inductance per unit length in the presence of an electron beam for the structure has been obtained considering the loss-free condition. These series inductance and shunt capacitance expressions are used for deriving the structure dispersion relation, and the temporal growth rate along with the estimation of RF output power and energy. Since the structure is azimuthally asymmetric, the symmetric TE and TM modes do not exist independently, thus, the two different modes excited in the azimuthally partitioned

structure are studied. The temporal growth rate associated with the two different modes has been calculated numerically. Further, to confirm the structure capable of generating bi-frequency; the simulation study has been performed in the presence of an electron beam. The obtained result through analysis and simulation is compared with results given in the literature. The relative error between them is below 5% which shows a good agreement. Furthermore, the effect of beam parameter variation on the temporal growth rate for two different modes associated with the different azimuthal sections has been appreciated computationally.